Invited contribution to the Special Edition of Curr Pharm Biotech titled
"The way down from single genes, and proteins to single molecules"

Data Reduction Methods for Application of Fluorescence Correlation Spectroscopy to Pharmaceutical Drug Discovery

*Lloyd M. Davis[a], Peter E. Williams[a], David A. Ball[a],
Kerry M. Swift[b], and Edmund D. Matayoshi[b]
[a]*Center for Laser Applications, University of Tennessee Space Institute, Tullahoma, TN 37388*
[b]*Abbott Laboratories, Abbott Park, IL 60064-6114*

Abstract:
Fluorescence methods are commonly used in pharmaceutical drug discovery to assay the binding of drug-like compounds to signaling proteins and other bio-particles. For binding studies of non-fluorescent compounds, a competitive format may be used in which the binding of the compound results in displacement of another fluorescently labeled ligand. Highly-sensitive measurements within nano-liter sized open probe volumes can be accomplished using a confocal epi-illumination geometry and thus key tools for such drug-binding studies include fluorescence correlation spectroscopy (FCS) and its related techniques. This paper reviews the general protocol for application of FCS to biomolecular compound-binding assays and it focuses on methods for the reduction of experimental photon count data to obtain the normalized autocorrelation function (ACF), on theoretical models of the ACF, and on statistical and systematic errors in the experimental ACF. Results from a detailed Monte Carlo simulation of FCS, which are useful for testing theoretical models and validating short-duration assay capabilities, are discussed. An illustrative example is presented on the use of FCS to assay binding of Alexa-488-labeled Bak peptide with Bcl-x_L, which is an intracellular protein that acts to protect against programmed cell death.

Keywords: fluorescence correlation spectroscopy; single-molecule detection; ligand-binding assay

1. INTRODUCTION

Fluorescence correlation spectroscopy (FCS) is a resourceful method for determination of the concentrations and kinetic and photophysical properties of solution constituents from measurements of fluorescence fluctuations, which arise when the number of molecules observed at any given time is down to the single-molecule level. Since its early inception [1-7], technological developments in single-molecule detection (SMD), confocal optics, and photonics during the early 1990's [8-17] have enabled FCS to become a practical tool in the biosciences [18,19], with second-generation instruments now commercially available [20]. One of the first commercial applications of FCS and SMD was for the assay of bi-molecular interactions for the pharmaceutical industry with the 1993 establishment of the company Evotech. A book that provides 22 reviews on various aspects and applications of FCS [21] and several other excellent reviews on FCS [22-24], which include practical information on experimental instrumentation, have recently been published.

In this paper, we focus on data reduction and analysis aspects of FCS and the application of FCS to the determination of interactions between pairs of bio-molecules [25]. Section 2 begins with a brief overview on the use of fluorescence techniques for pharmaceutical compound screening and it introduces fluorescence methods for competitive ligand-binding measurements, including those complementary to

FCS, such as methods based on fluorescence polarization and fluorescence brightness fluctuations. Section 3 reviews the methodology by which FCS and the normalized autocorrelation function (ACF) are used to assay compound binding, and discusses the theoretical functional forms used to curve fit the experimental ACF. Section 4 presents results from a Monte Carlo simulation of FCS. Section 5 discusses experimental means for acquisition of the ACF including algorithms for computation of the ACF from the individual times-of-arrival (TOAs) of detected photons. Section 6 reviews errors and signal-to-noise issues. Section 7 provides an example of the use of FCS to assay binding of a Bak peptide to the protein Bcl-x_L.

2. FLUORESCENCE DIAGNOSTICS FOR PHARMACEUTICAL COMPOUND SCREENING

The initial task in high-volume pharmaceutical compound screening is to sort through thousands of drug-like compounds from a library to find those that bind or interact with a target protein or bio-molecule, which has been identified from prior molecular-biology knowledge. Miniaturization of sample volumes to conserve reagents and homogeneous solution assay are generally preferable in the initial screening measurements [26]. The overall time for data collection may be reduced by multiplexing the initial measurements. For example, each sample may contain many different compounds, with each compound occurring in two or more different samples, and matching of the binding assay results may be used to identify the particular compound responsible for each positive binding result. Further measurements and research can then be performed on the identified compounds.

Fig. (**1**) illustrates typical data from a compound-screening run [27]. An experimental measure is made of the degree of binding to the target that occurs for any of the compounds within each sample. Systematic errors in the binding measure are oftentimes present. These may arise from many causes, including precipitation of solution components or adsorption onto surfaces, uncertainties in the concentrations of solution components, unwanted interactions between test compounds, and unaccounted sources of signal such as autofluorescence. Such errors account for apparent binding results that are less than 0%, or greater than 100%, as seen in Fig. (**1**). Nevertheless, it is still possible to identify many compounds that consistently yield apparent binding and that warrant further assays. However, these positive results are usually only expected to lead synthetic chemists toward new and better compounds. The success of the drug discovery/design process then depends on further medicinal chemistry and structural biology.

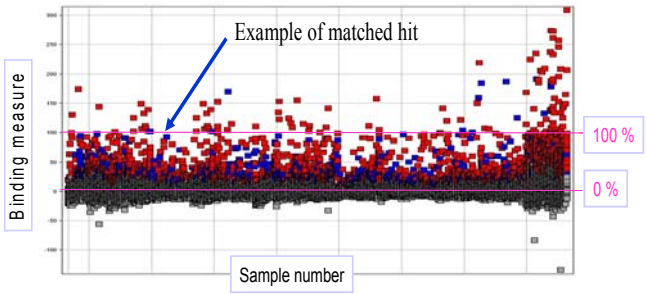

Fig. (**1**): Typical high-volume compound-screening results.

Fluorescence detection methods form the basis of many assays for the determination of whether interactions occur between the target bio-molecule and any of the drug-like compounds within each sample. Most importantly, fluorescence provides exquisite sensitivity down to the single-molecule level and requires only microliter sample volumes and nanomolar concentrations of components [14]. These features are particularly apparent in an experimental set-up that uses a confocal epi-illumination

geometry, in which a laser beam is focused by a high-numerical-aperture objective to a sub-micron waist for sample excitation, and in which fluorescence that is collected by the same objective is focused through a pinhole to limit the effective probe volume.

In order to test thousands of different drug-like compounds, including non-fluorescent compounds, with the same assay, a competitive binding strategy is generally employed [28]. First, a ligand that is known to bind to the target bio-molecule must be fluorescently labeled. Optionally, the bio-molecule itself may be fluorescently labeled using a distinct dye [29]. The labeled ligand and target bio-molecule solutions are mixed at concentrations appropriate to achieve approximately 50% bound ligand. Under these conditions, the fraction of binding is most sensitive to competitive binding by other agents. Then, if a drug-like molecule that can also bind to the target is added, some of the labeled ligand becomes displaced into free solution.

The labeled ligand may then exhibit a change in its fluorescence brightness, lifetime, or other spectroscopic properties. In the optional case that the target bio-molecule is also fluorescently labeled, the fluorescence signals from displaced ligands would no longer appear coincident with those from target bio-molecules. Coincidence detection techniques, such as the cross-correlation function [29], would then yield a very sensitive measure of labeled-ligand displacement, but at the drawback of additional chemistry to label the target. More generally, when the labeled ligand is displaced from the target, its rotational and/or translational diffusion become faster. In the first case, fluorescence polarization (FP) may be used to monitor rotational diffusion, and in the later case FCS may be used to monitor translational diffusion [30].

For Einstein-Stokes diffusion and approximately globular molecules of radius r, the translational diffusion scales as $1/r$, whereas the rotational diffusion scales as $1/r^3$. Hence the rotational diffusion is a more sensitive indicator of binding, scaling as $1/MW$, where MW is the molecular weight, whereas translational diffusion only scales as $1/MW^{1/3}$. In order to distinguish two components by FCS, their translational diffusion times must differ by a factor of at least 1.6 [31] and hence the target bio-molecule must be at least 4 times the size of the ligand. On the other hand, FP can only monitor rotational diffusion changes if the fluorescent label is rigidly bound to the ligand. It may be advantageous to measure the time resolved fluorescence anisotropy [32]. Oftentimes the label is bound to the ligand with partially restricted motion, but is free to rotate about a particular axis, such as around a covalent link. In such cases, the time-resolved fluorescence anisotropy would exhibit multiple exponential decay components, whereas the time-averaged or "steady-state" anisotropy would be dominated by the faster component, which is not altered by the binding of the ligand to the bio-molecule. Further, if FP is to successfully monitor changes in ligand-target binding, the fluorescence lifetime of the label must be longer than the slow-axis rotational lifetime of the ligand when it is bound to the target bio-molecule. With the above considerations, FP and FCS are best considered as complementary rather than competing tools for the assay of competitive binding of drug-like compounds to a target [30]. It should be remarked that polarization-sensitive FCS can also be used to determine rotational diffusion [4].

Other complementary methods, which are particularly helpful when mass changes due to binding are not detectable solely by FP or FCS, include techniques that are related to FCS in that they also measure fluctuations within the data set. Assays based upon the histogram of photon numbers within successive bins of fixed width, which are applicable when binding results in at least a 2-fold change in fluorescence brightness, include analysis of the photon counting histogram (PCH) [33] and fluorescence intensity distribution analysis (FIDA) [34]. These two techniques are similar, but make different approximations in the derivation of a theoretical model for curve fitting of the histogram and hence have different experimental operating conditions. They can resolve fluorescence fluctuations with different mean brightness values but not with different timescales, whereas the normalized ACF used in FCS captures

information on the timescales but not on the brightness values of the fluctuations. Fluorescence intensity multiple distribution analysis (FIMDA), in which a set of photon-count histograms is collected for a selection of bin widths, captures information on both the timescales and the brightness values of the fluorescence fluctuations [35]. Fluorescence intensity and lifetime analysis (FILDA) captures information on the fluorescence lifetimes and brightness values of solution constituents. Many of these other complementary techniques, which may be considered superior in that they capture greater information content than FCS, are reviewed and referenced in the next article in this volume [36], and the present paper instead focuses on the capture and analysis of the normalized ACF, which is defined as

$$g(\tau) = \frac{\langle F(t)F(t+\tau)\rangle}{\langle F(t)\rangle\langle F(t+\tau)\rangle}, \tag{1}$$

where $F(t)$ is the fluorescence detector photon count rate at time *t*, and the angular brackets denote an average over all times, whereby

$$\langle F(t)F(t+\tau)\rangle = \lim_{T\to\infty} \frac{1}{2T}\int_{-T}^{T} F(t')F(t'+\tau)\,dt'. \tag{2}$$

3. FCS METHODOLOGY IN LIGAND-BINDING MEASUREMENTS

In the determination of ligand-target interactions, FCS is used to monitor the equilibrium reaction

$$\text{[free labeled-ligand]} + \text{[target]} \leftrightarrow \text{[bound labeled-ligand]}, \tag{3}$$

where the dissociation constant of the reaction

$$K_d = \frac{\text{[free labeled - ligand][target]}}{\text{[bound labeled - ligand]}}, \tag{4}$$

determines the ratio of molar concentrations of the species. In a typical assay, a series of normalized ACF is recorded for a constant total concentration of labeled ligand with a logarithmically increasing concentration of target, which is titrated into the sample in negligible volume aliquots so that the total concentration of fluorescently labeled molecules remains approximately constant. Each ACF of the series is curve fit to a theoretical model, which typically includes 2 components with diffusion-timescale parameters that correspond to the free and bound labeled-ligands of reaction (3).

For a multi-species sample and diffusional transport of molecules through an assumed 3-dimensional (3-D) Gaussian-shaped probe-region, with $1/e^2$ radii ω_0 and z_0 in the transverse and axial directions, an analytical model for the normalized ACF, derived in the early FCS literature [5-7], can be formulated as [37]

$$g(\tau) = 1 + \frac{\xi(\tau)}{N_{\text{tot}}}\left(1 - \frac{I_B}{I_{\text{tot}}}\right)^2 \sum_j \phi_j \left(\frac{1}{1+\tau/\tau_j}\right)\left(\frac{1}{1+(\omega_0/z_0)^2\tau/\tau_j}\right)^{1/2} \tag{5}$$

where

$$I_{\text{tot}} = \sum_j I_j + I_B, \tag{6}$$

is the total count rate, composed of the count rates from each species I_j plus the uncorrelated background count rate I_B, ϕ_j is the weighting factor for the *j*-th species, and is given by

$$\phi_j = \frac{\Phi_j N_j / N_{\text{tot}}}{\left(\sum_j \Phi_j N_j / N_{\text{tot}}\right)^2}, \tag{7}$$

where Φ_j is the fluorescence brightness of the *j*-th species, and N_j is the number of molecules of the *j*-th species in the sampled volume, with $N_{\text{tot}} = \sum_j N_j$, and

$$\tau_j = \omega_0^2 / 4D_j \,, \tag{8}$$

where D_j is the translational diffusion coefficient for the j-th species. In equation (5), the factor

$$\xi(\tau) = 1 + (\overline{T}/1-\overline{T})e^{-\bar{k}_T\tau} \tag{9}$$

is an approximate correction for triplet kinetics and is of the same form as Eqn. (6.6.18) of Ref. [5] for the case of molecules being removed from solution by a chemical reaction. Here $\bar{k}_T$ is the mean effective rate at which molecules are driven into the non-fluorescent triplet state (not the rate of depopulation of the triplet state as stated in [37]), and $\overline{T}$ is the mean effective fraction of the fluorophores in the observation volume that are in their triplet states [38].

For two species, Eqn. (5) is of the functional form

$$g(\tau) = 1 + \left(1 + ae^{-b\tau}\right)\left[\left(\frac{c_1}{c_1 + c_2}\right)\left(\frac{1}{1+d_1\tau}\right)\left(\frac{1}{1+d_1 e\,\tau}\right)^{1/2} + \left(\frac{c_2}{c_1 + c_2}\right)\left(\frac{1}{1+d_2\tau}\right)\left(\frac{1}{1+d_2 e\,\tau}\right)^{1/2}\right]. \tag{10}$$

When the curve fit to the experimental ACF is performed, as many parameters as possible in Eqn. (10) are held fixed at values obtained from prior calibration experiments, while the species contributions of the free and bound labeled-ligand components (c_1 and c_2) are adjusted for optimal fit. Examples of parameters typically held fixed include the 'confocal parameter', e, which is the ellipticity of the probe volume ω_0 / z_0 and which is determined from a curve fit of a known-fluorophore ACF, and the diffusion-timescale parameters (d_1 and d_2), which can be obtained from the curve fits of ACFs from either ends of the titration series. Oftentimes the first two or three points in the experimental ACF, which are influenced by detector deadtime and afterpulsing, are omitted in the curve fit.

Random and systematic experimental errors and approximations in the theoretical model used to curve fit the ACF introduce errors into each of the deduced species concentrations, but these errors are to some extent correlated such that the fractional contributions $c_j/(c_1+c_2)$ have tolerable error. A curve fit to the plot of the deduced bound fraction versus target concentration can then be used to obtain the dissociation constant K_d of Eqn. (4).

For high-volume compound screening, or to assay binding of a particular non-fluorescently-labeled ligand, the concentrations in reaction (3) are such that about 50% of the labeled ligand is initially bound. The ACF is recorded and then recorded again after the mixture of test reagents is added, or it is recorded for logarithmically increasing concentrations of the particular unlabeled ligand. If competitive binding occurs, reaction (3) is driven to the left. The ACF is curve fit to Eqn.(10), with bound and free species contributions as adjustable parameters, from which the bound fraction is deduced. As the concentration of unlabeled ligand is logarithmically increased, increased competitive binding results in a decrease in the bound fraction from 50% to as little as 0%. Hence if the assay is to be successful, the shape of the experimental ACF must be measurably altered as the bound fraction decreases from 50% [31].

Excitation saturation, triplet state build-up, and photodegradation, are factors that must be considered in many FCS ligand-binding measurements. Reagents such as mercaptoethylamine may be added to solution to enhance the photostability or quench the triplet manifold of the fluorophore [39]. Laser excitation power may be reduced to minimize the contribution of these effects to the apparent distortion of the experimental ACF [38], but the signal to background is then decreased and the fluorescence counts per molecule and hence noise in the ACF is increased (see section 6). Oftentimes, the approximate correction factor of Eqn. (9) must be included in the curve fitting function for interpretation of experimental ACF. However, Eqn. (9) does not account for the concomitant saturation effects that usually occur when triplet-state photo-physics are present. Saturation effects have been included in an approximate model for the case of two-photon excitation [40], although the observed triplet fractions

$\overline{T}/(1-\overline{T})$ in FCS experiments with two-photon excitation are typically smaller than in those with one-photon excitation.

Another cause of ACF distortion, which arises from departure of the sample volume profile from the assumed 3-D Gaussian shape, has been addressed by numerical calculation of the focused-laser-beam-profile and optical-collection-efficiency-profile factors that contribute to the sample volume profile, and by numerical integration to obtain a numerical fitting function [41]. However, from a practical perspective, numerically-based calculation of a fitting function would be more useful if saturation, triplet kinetics, and photodegradation were also included.

4. MONTE CARLO SIMULATIONS OF FCS

In order to facilitate the study of realistic experimental conditions, such as triplet crossing, photobleaching, excitation saturation, detector dead time, and optical misalignment, to evaluate the effects of systematic and random errors in the ACF with short duration acquisition times, and to facilitate comparison of different data analysis strategies, a Monte Carlo simulation of single-molecule detection (SMD), FCS and fluorescence cross correlation spectroscopy (FCCS) has recently been developed [25]. The simulation is quite different from those that add random-number generated noise to a theoretical model ACF curve [31], but is an *ab initio* approach like those of Refs. [42-44], which follow the trajectories of individual molecules as they are carried through the probe volume. However, a key difference compared to prior simulations [42-44] is that the new code does not use a fixed iteration time step but generates the exact time of arrival (TOA) of each detected photon (as a double precision real number in units of seconds). The photon TOAs are then available for any chosen measurement and data reduction scheme. The new simulation uses an algorithm in which molecule locations are confined to a discrete grid and time increases continuously for all processes except molecule transport. Unlike Ref. [43], molecules may enter or leave the simulation volume by diffusion or flow. The simulation can model one or two independently aligned laser excitation beams, one or two single photon detectors, several different chromophore types, and several particle types with different mobilities, labeled by specified numbers of the defined chromophore types and has been recently extended to include modeling of Forster resonance energy transfer. The execution time depends on input parameters and photon detection rate, but is of the order of 100 s for a 1-10 s experiment, including the calculation of the normalized ACF from the photon TOAs described in section 5 and more. The code uses multiple threads, with key parts written in C and compiled using the Intel compiler [45].

Fig. (**2**) shows a screen shot during program execution of the simulation interface, which is written in LabView (National Instruments: http://www.ni.com/).[1] As an example of the use of the simulation to investigate saturation effects concomitant with triplet photophysics, Fig. (**3**) presents ACF from simulations using parameters listed in Table 1, and the simulation geometry illustrated in Fig. (**2**), which models the Zeiss Confocor 2 with parameters similar to those of Ref. [20].

[1] An example of the simulation will be made available at http://www.utsi.edu/ldavis.

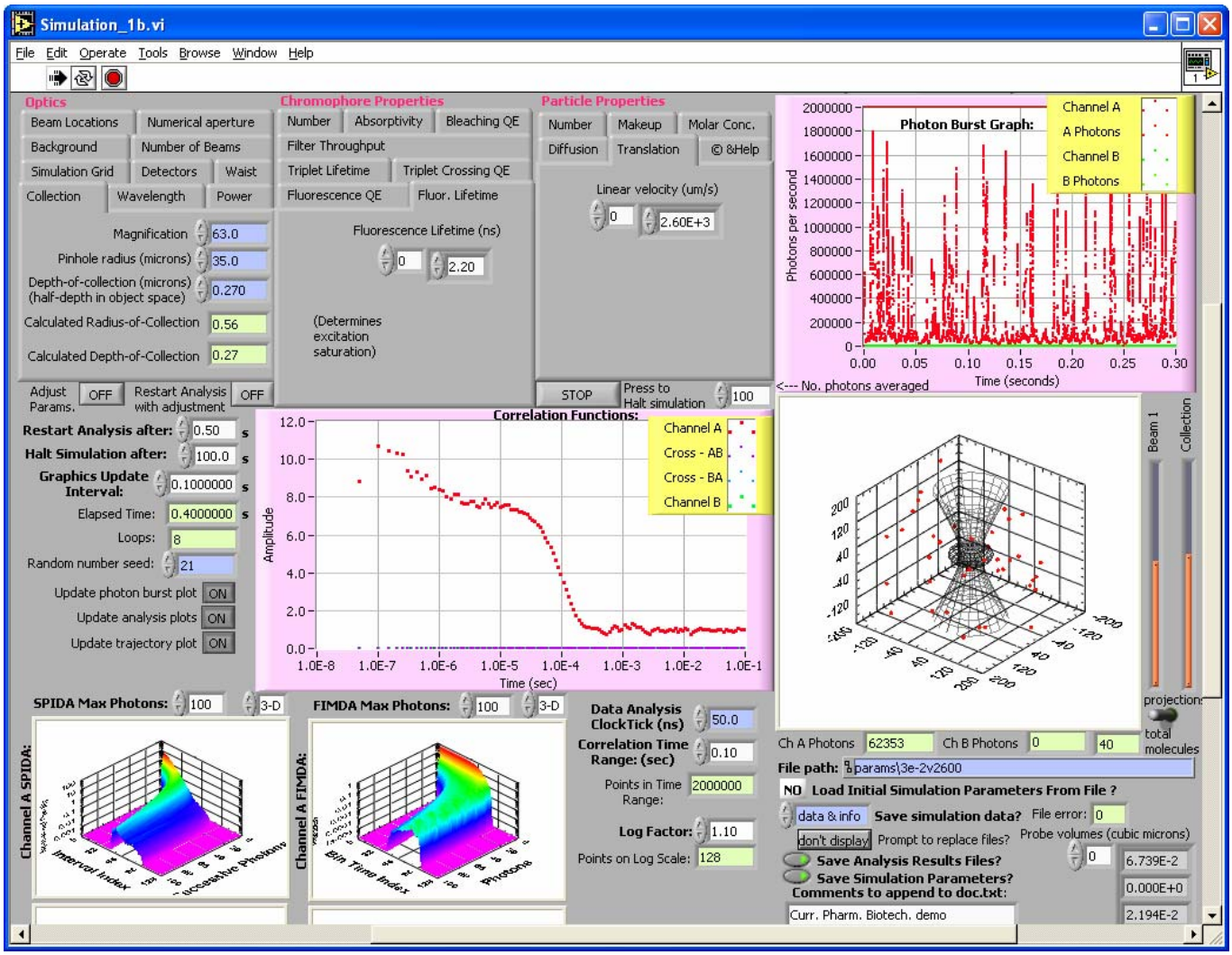

Fig. (**2**): Screen shot of the computer simulation of SMD and FCS, as described in the text, after only 0.3 s of a 100 s simulation of result E of Fig. (**3**).

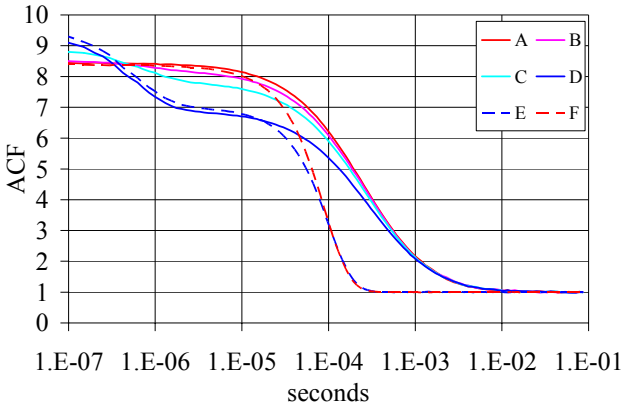

Fig. (**3**): Normalized ACF from Monte Carlo simulation of FCS with triplet crossing and flow, using parameters listed in Table 1.

Table 1: Simulation parameters used to generate the ACFs shown in Fig. (**3**), which illustrate the effects of varying triplet crossing and sample flow. The photobleaching rate is set to zero in order to allow unambiguous interpretation of the changes to the ACF.

Parameter		**Value**
Collection Time (s)		100
Simulation Grid Resolution (μm)		0.001
Numerical Aperture, *NA*		1.2
Magnification		63
Pinhole Radius[a] (μm)		35
Depth-of-Collection[a], z_0 (μm)		0.27
Laser Wavelength, λ (nm)		488
Laser Beam Waist[b], ω_0 (μm)		0.26
Laser Excitation Power (μW)		50
Background Count Rate[c], I_B (s^{-1})		600
Spectral Filter & Optics Throughput		0.6
Detector Quantum Efficiency		0.65
Detector Dead Time (ns)		35
Molar Absorptivity (cm^{-1} $mole^{-1}$)		67000
Molar Concentration (moles $liter^{-1}$)		10^{-9}
Diffusion Time[d], τ_1 (μs)		307
Data Analysis Clock Period[e] (ns)		50
Fluorescence Lifetime (ns)		2.2
Triplet Lifetime (μs)		1
Fluorescence Quantum Efficiency		0.9
Bleaching Quantum Efficiency		0
Triplet Crossing Efficiency	A, F	0
	B	0.003
	C	0.010
	D, E	0.030
Flow Time[f], τ_F (μs)	A–D	∞
	E, F	100

[a] $e^{-1/2}$ radius of assumed Gaussian collection efficiency profile in image space.
[b] Defined before Eqn. (5).
[c] Defined in Eqn. (6).
[d] Defined in Eqn. (8).
[e] Defined as `clock` in Section 5.
[f] $\tau_F = \omega_0/v$, where v is the flow velocity.

The simulations illustrate the effects of increasing triplet crossing probability for constant laser power for a single species. Note that the correction factor in Eqn. (9) is greater than 1 for all values of τ. As seen in Fig. (**3**), when triplet effects occur, the normalized ACF is increased for small values of τ and decreased for larger τ values. Accordingly, a curve fit to Eqn. (5) for a single species would yield a value of N greater than the actual value. Nevertheless, for a solution containing two species, the fractional contributions $c_j/(c_1+c_2)$ obtained from a curve fit to Eqn. (10) would still be expected to be correct provided that the effective triplet parameters a and b are the same for each species. Also, the dashed

curves in Fig. (**3**) illustrate that a flow or translation of the sample does not alter the amplitude of the ACF if there is no triplet crossing [7], but when triplet crossing occurs, flow can replenish molecules that are in the triplet state with ground state molecules (as is well known in the operation of dye lasers), and hence can alter the ACF amplitude and the observed triplet fraction. Flow can similarly be used to replenish photobleached molecules [29]. Although such effects are well known, the simulation is useful for quantification of the effects on the ACF for the chosen experimental conditions.

5. EXPERIMENTAL AUTOCORRELATION FUNCTION ACQUISITION

In this age of continually advancing computational power, software options for on-line calculation of the ACF from experimental data are now replacing traditional hardwired correlators. Nevertheless, the first digital photon correlators, pioneered in the 1970s by Malvern Instruments for dynamic light scattering [46], used simple processing circuits that provide the basis for our present day software algorithms. These calculated the "clipped" ACF by first counting photons into bins of equal time widths, then reducing the numbers of counts in the successive bins, I_j, j = 0, 1, 2, …, to single-bit values, either I_j = 0, or 1 if the number of counts was above a preset threshold or clip level, and then evaluating the correlation values

$$A_m = \sum_j I_j \times I_{j+m} , \tag{11}$$

which approximate Eqn. (2), by use of shift registers and simple logic for the single-bit multiplications. By the 1980s it became practical to carry out a similar process in software with a personal computer (PC) linked to a digital oscilloscope, with software thresholding of the digitized detector pulses to yield a sequence of zeros and ones, and with experiment duration limited by the digital oscilloscope memory. In early SMD experiments [47], the voltage pulses from a time-to-amplitude converter were digitized using a PC-based 1 MHz analog-to-digital converter, and the number of "zeros" between successive photon pulses were counted in software to determine the time-of-arrival (TOA) of each photon to a precision of 1 microsecond.

The recording of the TOA of each detected photon provides the most complete experimental data acquisition modality for SMD and FCS, and may now be directly accomplished with reduced memory requirements, without recording each of the "zeros" between photons. Ref. [48] describes a custom PC-based data acquisition card for full access to the detected photon sequence with 40 MHz timing. In our recent work, we have used a PC-based National Instruments PCI-6602 counter/timer card (80 MHz clock), or a Picoquant TimeHarp 200 PC-based card with "time-resolved-time-tagged" option (10 MHz timing), or decoding of the raw data files from the Zeiss Confocor 2 data acquisition system (20 MHz timing) to gain access to the sequence of photon TOAs. Evaluation of the ACF and various other data reduction strategies, including FIMDA [35], can then be performed using algorithms that directly process the list of photon TOAs as they are acquired. Fig. (**4**) illustrates a simple algorithm, reported in Ref. [47], by which the un-normalized ACF at a delay of `m` clock cycles `A[m]`, equivalent to A_m of Eqn. (11), may be accumulated in real time as a histogram of cumulative delay times, between the photon TOAs `t[i]`, of a series of `np` photons. Ref. [49] includes a similar algorithm for accumulation of cross-correlation functions (CCFs). Fig. (**4**) also illustrates the accumulation of a family of histograms `S[k][m]` of delay times between `k+1` successive photons, which we have termed "successive photon interval density analysis" (SPIDA) [44], and which, like FIMDA, captures information on both the temporal durations and brightness values of photon bursts. When equivalently normalized, the sum of all SPIDA curves yields the ACF. An example of a SPIDA plot is shown at the bottom left of Fig. (**2**).

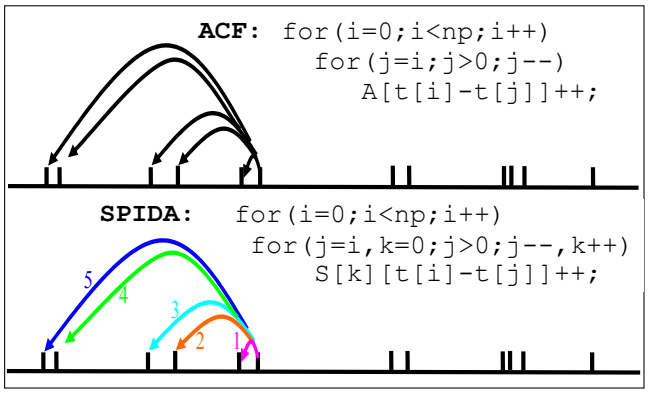

Fig. (**4**): Algorithm for accumulation of the ACF and SPIDA from photon TOAs.

Values of the un-normalized ACF at linearly spaced delay values, `A[m]`, may be averaged to obtain the values at a smaller number of arbitrarily-spaced delay values. In our work, the ACF is calculated out to a pre-specified maximum delay of `m=limit-1` (typically 10^5—10^6 clock cycles), and a logarithmic spacing of points with arbitrary slope is achieved by definition of an array of logarithmically-spaced delays `D[n]`, with values increasing from `0` to `limit-1` by use of code similar to the following C code:

```
for(m=n=0,f=1.0;m<limit;n++,f*=logfactor,m+=(int)f)D[n]=m;
D[n]=limit-1;
```

where `logfactor` is an arbitrary pre-specified floating point value > 1.0 that determines the slope. Note that the un-normalized ACF values at the logarithmically-spaced delays `AL[j]` may be directly accumulated into an array of dimension `n+1` (typically about 100—500) as follows: When the `i`-th photon TOA `t[i]`, is received, if its value is greater than `limit`, the `n+1` values of `AL[j]` are updated by code similar to the following:

```
k=i-1;AL[0]++;
for(j=1;j≤n;j++){d=t[i]-D[j];for(l=k;t[k]>d;k--);AL[j]+=(l-k); }
```

At the completion of the stream of the `np` photons, in which `t[0]=0` and `t[np]≤T`, where `T` is the duration of the experiment in clock cycles, the number of clock delay values that contribute at each value of `j` must be accounted for by use of code similar to the following to obtain the normalized ACF `gL[j]`:

```
for(j=1;j≤n;j++){gL[j]=AL[j]/(AL[0]*AL[0]*(T-limit)*(D[j]-D[j-1]));
tL[j]=clock*0.5*(DL[j-1]+DL[j]+1);}
```

where `clock` is the period of the clock cycle in seconds (i.e., the width of a single bin for the I_j values of Eqn. (11)), and `tL[j]` are the delay times in seconds of the logarithmically-spaced ACF values `gL[j]`. Fig. (**5**) shows the number of linearly-spaced ACF values `0.5*(DL[j-1]+DL[j]+1)` that are effectively averaged versus time delay `tL[j]` for a 20 MHz clock and a value of `logfactor=1.1`, as used in the calculation of the ACFs shown in Figs. (**2**) and (**3**).

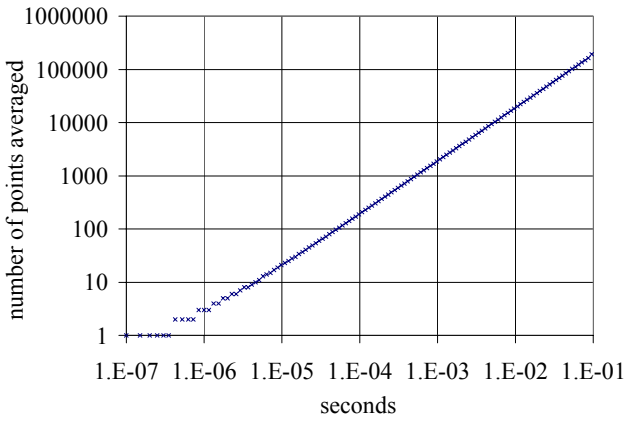

Fig. (**5**): The number of linearly-spaced ACF values that are effectively averaged versus time delay, with the accumulation of 128 logarithmically-spaced ACF values between 50 ns and 0.1 s.

6. ERRORS IN THE ACF

In the commonly-used multi-tau hardware correlators available from ALV-Laser (www.alvgmbh.de) or Correlator.com (www.correlator.com), in order to determine the ACF over a wide range of time delays that are approximately equally spaced on a logarithmic scale, the photon counts in adjacent linearly spaced bins are repeatedly grouped together to form counts in many sets of bins of temporal widths that increase by factors of 2 from the prior set, and Eqn. (11) is evaluated for each set to determine the ACF at different sets of delay values, as described in more detail in Refs. [43, 46, 50]. However, the use of broadened bin widths (which result from many adjacent bins being added) causes the fluorescence fluctuations to be smoothed, and hence it causes the measured ACF, at those delay values that use the broadened bin widths for their determination, to be smoothed. The smoothing is equivalent to convolving the ACF with a triangular filter function, which is the autocorrelation function of the rectangular bin width. The resultant ACF at the longer time delays will be biased (as described at www.correlator.com/mt64.htm) unless the ACF has already decayed to zero at those delay values. By comparison, the direct evaluation of the ACF from the photon TOAs described in section 5 uses the same narrowest bin width for all delay points of the ACF, and hence is expected to exhibit negligible bias due to smoothing of the fluorescence signal.

A further source of bias can occur for finite duration experiments. Whereas the definition of the ACF given in Eqns. (1) and (2) involves integrals over infinite durations, evaluations based on finite duration experiments are only estimates of the true ACF, just as a sample mean is merely an estimate of the population mean. From the days before FCS was invented, the estimate of the normalized ACF from finite data sets, was found to be biased [51]. The bias scales inversely with the number of bins M that contribute to the sum in Eqn. (11) and is usually not observed. However, for a multi-tau correlator, M can be low when the bin widths are broad, when the correlation is evaluated for a moderate time delay, and when the acquisition time is relatively short [50].

Soon after FCS was invented, Koppel analyzed the statistical and systematic errors at any given single point in the experimental ACF in order to understand and improve the factors that govern signal-to-noise [52]. He found that the critical parameter that governs the statistical accuracy (when background fluorescence is negligible) is not the total photon counts per correlation time, but rather the total photon counts per single molecule per correlation time, which is independent of the concentration. Koppel's derivation was later extended to consider conditions closer to those of the typical FCS experiment [53, 54]. Also, his treatment was extended in an effort to determine the statistical error bars at all points in the normalized ACF [43, 50]. It was found that weighted curve fitting of the ACF with use of the error bars

can improve the parameter estimation for FCS. We have found that when the ACF is calculated directly from the photon TOAs, the major contribution to the difference in precision of different points in the ACF is the number of linearly-spaced ACF values that are effectively averaged, as illustrated in Fig. (**5**).

For short data acquisition times, as would occur in high-volume compound screening applications, different methods for calculating the ACF from the photon TOAs can result in different statistical errors, and systematic errors or bias other than those described above can also occur. Here we compare four different ways of estimating the normalized ACF from short duration finite data sets, which have been generated by the simulation to avoid experimental effects such as laser drift. Fig. (**6**) illustrates the four formulae for evaluating the normalized ACF, which we have implemented directly from the photon TOAs. In g_0, there is an attempt to correlate data with other data outside the range of the experiment. The evaluation can still be performed if the out-of-range data is assumed to take some value, such as zero. In g_1, it is recognized that the ACF is to be evaluated out to a time τ = T, and hence accumulation of the ACF waits until after a duration T of the data has passed. This is the method usually used in our simulation to accumulate the ACF (e.g., in Fig. (**2**), center), because of its simplicity, and is that of the code fragments given in section 5. However, it does not efficiently utilize the data. In g_2, different wait times τ are used before evaluation of each point in the ACF. Also, different values of the summed intensity must be used to normalize the ACF at each point τ. In g_3, symmetrical normalization is used, thereby requiring three different summations for each point τ.

$$g_0(\tau) = \frac{T\sum_{t=0}^{T} I(t)I(t-\tau)}{\left[\sum_{t=0}^{T} I(t)\right]^2}, \tau = 0,..., \mathrm{T}$$

$$g_1(\tau) = \frac{(T-\mathrm{T})\sum_{t=\mathrm{T}}^{T} I(t)I(t-\tau)}{\left[\sum_{t=\mathrm{T}}^{T} I(t)\right]^2}, \tau = 0,..., \mathrm{T}$$

$$g_2(\tau) = \frac{(T-\tau)\sum_{t=\tau}^{T} I(t)I(t-\tau)}{\left[\sum_{t=\tau}^{T} I(t)\right]^2}, \tau = 0,..., \mathrm{T}$$

$$g_3(\tau) = \frac{(T-\tau)\sum_{t=\tau}^{T} I(t)I(t-\tau)}{\left[\sum_{t=\tau}^{T} I(t)\right]\left[\sum_{t=\tau}^{T} I(t-\tau)\right]}, \tau = 0,..., \mathrm{T}$$

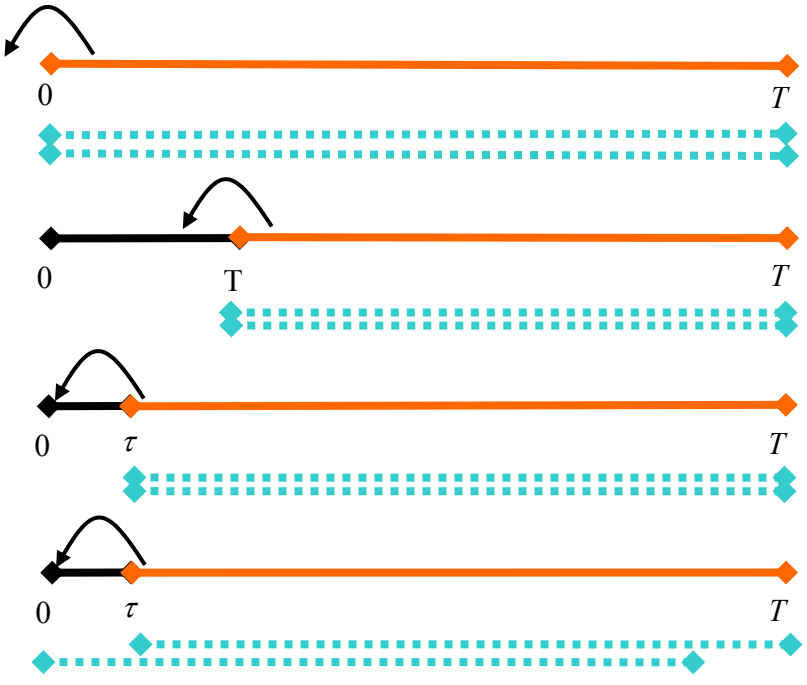

Fig. (**6**): Comparison of four methods for estimation of the ACF from finite duration data sets. The solid lines at right illustrate the time range of the summations in the numerators of the equations at left. The blue dashed lines illustrate the time ranges of the summations in the denominators, used to normalize the ACF.

For 0.2 s simulations of FCS using sulforhodamine 101 in water with the Confocor 2 geometry of Fig. (**2**) and evaluation of the ACF out to τ = 0.1 s, we find that g_0 yields biased estimates of the ACF in that the average of 100 ACFs from different 0.2 s simulations does not approach the ACF from a 100 s

simulation, particularly at the longer dwell times, as seen in Fig. (7a). We find g_1 yields unbiased estimates, but the spread in ACFs is considerably greater, as seen in Fig. (7b). In particular, the arrows in Fig. (7b) indicate considerable uncertainty in the width of the ACF.

Note that the errors at nearby points in each ACF estimate are correlated, so that the ACF from an individual 0.2 s simulation may have faster or slower width, but on average is unbiased. The fact that errors at nearby points in the ACF are not independent but are correlated means that although the use of error bars at each point in the ACF for weighted least-squares fitting of the ACF may improve the parameter estimation, it will never provide a statistically rigorous means of analysis, because least-squares curve fitting implicitly requires each data point to be statistically independent.

We find g_2 and g_3 also yield unbiased estimates, but they exhibit considerably less fluctuations in their widths than g_1, as may be expected from the more efficient use of data. We find that the symmetrical normalization in g_3 yields smaller errors than g_2 in the tail of the ACF, at the arrow of Fig. (7c), as has been reported elsewhere [55]. Also, by comparing Figs. (7c) and (7d), we see that evaluation of the ACF at fewer points by averaging the g_3 values at a larger numbers of adjacent τ values, corresponding to a larger value of `logfactor` and steeper slope in Fig. (7c), leads to less point-to-point fluctuations in an individual ACF.

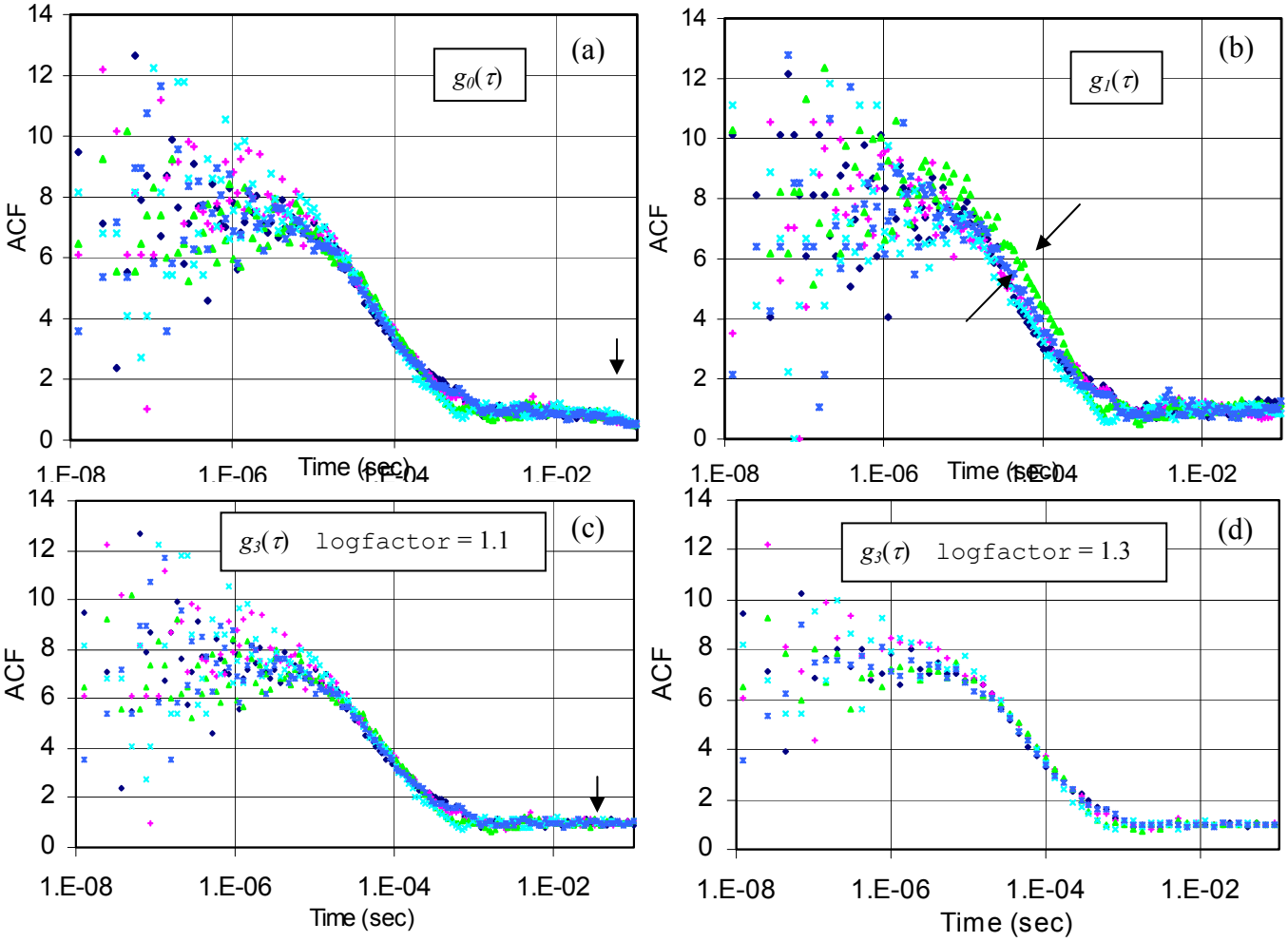

Fig. (7): Comparison of the ACF obtained from the same set of five different 0.2s simulations, as evaluated by four different methods discussed in the text.

Finally, Fig. (**8**) shows that contrary to the case of the multi-tau correlator discussed in Ref. [50], the g_3 estimate of the ACF from short duration experiments remains unbiased, even down to 0.2 s collection times, being within the random errors exhibited by the ACFs from several different 20 s simulations. The lack of bias holds even for a slow diffusion coefficient of 4×10^{-7} cm^2/s, which results in marked variation of the photon bursts, photon counts and ACF generated by different 0.2 s simulations.

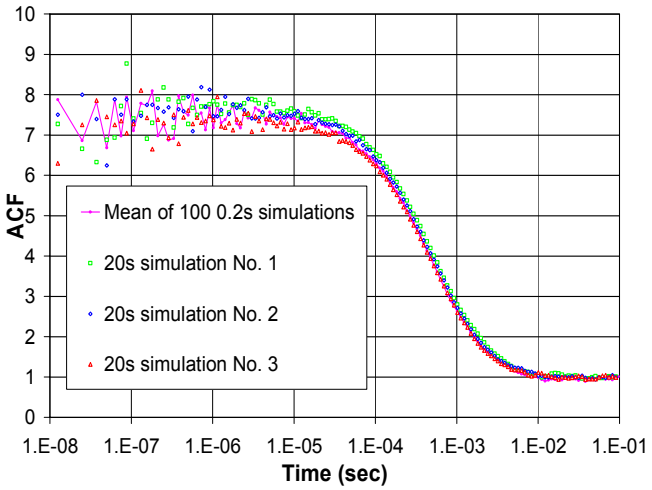

Fig. (**8**): ACFs calculated from simulated photon TOA data exhibit no bias with short acquisition times. Simulation parameters are similar to the experiments of Ref. [50], but with only a 0.2 s rather than 3-30 s acquisition time, namely 2.5 MDa dextran molecules, in this case labeled by sulforhodamine 101, ω_0 = 0.5 μm, yielding τ_D = 3125 μs, 20 μW laser power resulting in a fluorescence count rate of about 2800 counts/s, no triplet crossing, bleaching, background, or detector dead time.

7. EXAMPLE APPLICATION TO BCL-X_L

Because of its implication in a wide range of clinical disorders, including Cancer, autoimmune diseases, viral infections, and neuro-degenerative disorders, Bcl-x_L may be a useful signaling protein molecule to target for drug discovery efforts. Bcl-x_L is a protein from the Bcl-2 family that acts to protect against cellular apoptosis by complexing with pro-apoptotic Bcl-2 proteins, such as Bax, Bak, Bid, and Bad [56]. The latter stimulate mitochondrial release of cytochrome c, which activates caspases that in turn are the executioners of programmed cell death. Researchers at Abbott Laboratories have labeled a synthetic 16-residue Bak peptide with the fluorophore Alexa-488 from Molecular Probes and have determined the structure of the Bcl-x_L + Bak-ligand complex [57]. The fluorescently-labeled Bak peptide binds to the 20 kilo-Dalton Bcl-x_L protein and hence may be used in competitive binding assays of drug-like molecules that target Bcl-x_L.

Fig. (**9**) shows the results of a binding isotherm titration obtained using FP measurements. The total concentration of labeled Bak remains fixed at 1.1 nM and as the concentration of Bcl-x_L is increased, the labeled Bak becomes maximally bound and the steady state fluorescence anisotropy increases to an asymptotic value of 0.14. A curve fit to the data yields a dissociation constant, defined by Eqn. (2), of K_d = 2.3 nM, i.e., the ligand becomes 50% maximally bound for a Bcl-x_L concentration of about 2.3 nM. Although FP measurements are possible in a confocal-epi-illumination experiment, the data in Fig. (**9**) were obtained with 2 milliliter sample volumes and a measurement time of 15 seconds per data point using an Abbott clinical diagnostics instrument and with a sample temperature of 35 °C [58]. On the other hand, FCS invariably employs a femtoliter probe volume and hence a much smaller sample volume, but longer data acquisition times are generally necessary to acquire statistically significant data.

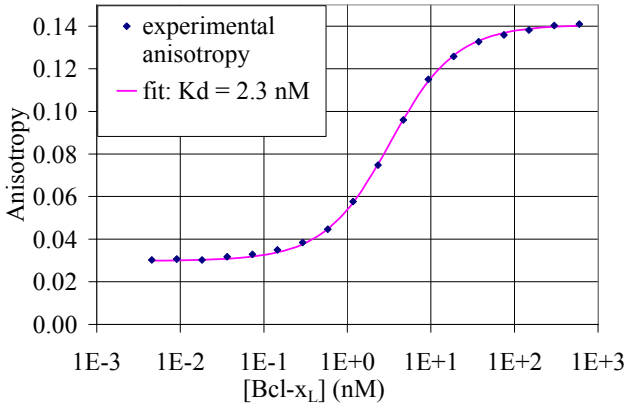

Fig. (**9**): FP assay of binding isotherm titration shows fluorescence anisotropy versus Bcl-x_L receptor protein concentration for a constant 1.1 nM concentration of Alexa-488-labeled Bak.

Fig. (**10**) shows an example of a 0.1 s section of photon bursts together with the normalized ACF collected in a 30 second experiment from a micro-liter-sized aliquot of sample at 21 °C by the Zeiss Confocor 2 FCS instrument. The graphs shown in Fig. (**10**) were numerically calculated from the photon TOAs obtained from the Confocor 2 raw data file, as discussed in section 5. The photon bursts include both slow and fast bursts, corresponding to bound and unbound fluorescent ligands. The ACF calculated from the TOAs exactly equals the ACF presented by the Zeiss Confocor 2 instrument for the initial delay values, and for all delay values the curves are in excellent agreement for the range of values of the parameter `logfactor`, which determines the density of logarithmically-spaced points in the calculated ACF.

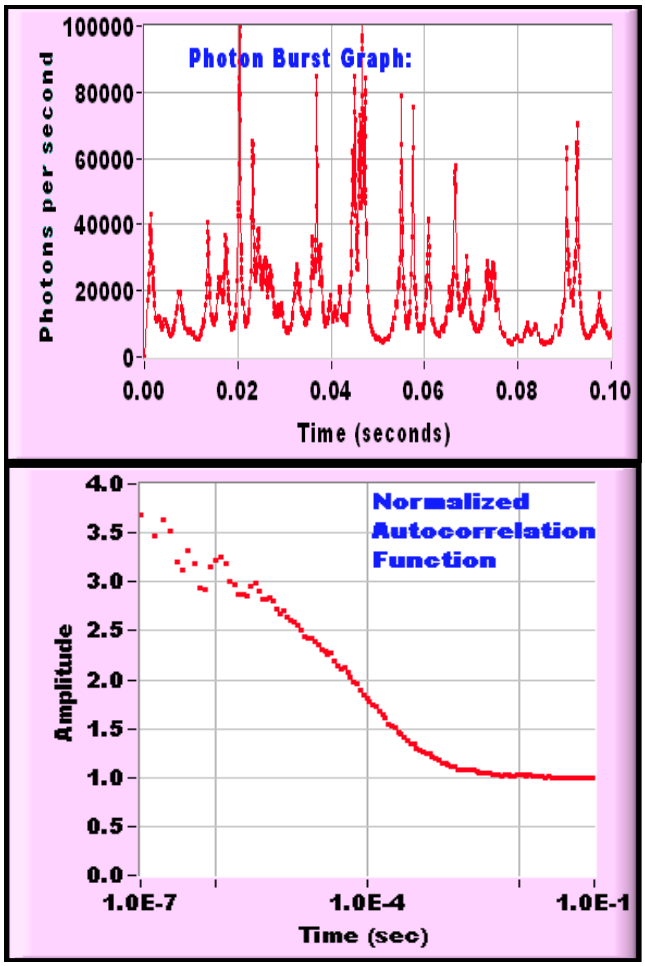

Fig. (**10**): A short section of the photon bursts (top) and the normalized ACF (bottom) calculated from the photon TOAs obtained from the Zeiss Confocor 2.

Three independent FCS measurements, each for 30 seconds of acquisition time, were performed at each point of the binding isotherm titration of Fig. (**9**). The normalized ACFs acquired by the Zeiss Confocor 2 instrument were fit using the Zeiss Confocor 2 software to a two-diffusion component model given by Eqn. (10), with fixed confocal parameter, fixed bound and free diffusional residence times, and adjustable triplet parameters, as illustrated in the screen shot in Fig. (**11**).

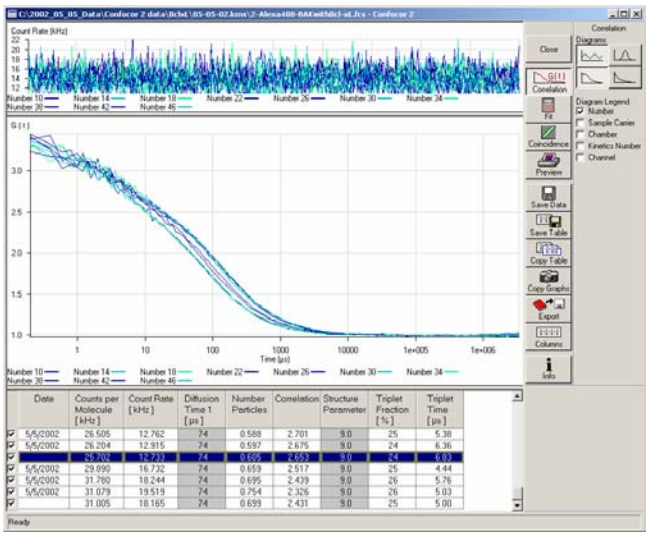

Fig. (**11**): A screen shot of the Zeiss Confocor 2 software for curve-fitting the ACF.

The percentage of the ACF component with slower 146 μs diffusional residence time $c_1/(c_1+c_2)\times 100\%$, which corresponds to labeled Bak peptide bound to Bcl-x_L, as obtained from an unweighted nonlinear curve fit of the normalized ACF, is plotted in Fig. (**12**). The total concentration of labeled Bak remains fixed at 1.1 nM and as the concentration of Bcl-x_L protein is increased, the labeled Bak becomes 100% bound. Also shown in Fig. (**12**) is the total fluorescence count rate, which decreases to 83% of its initial value as the labeled Bak becomes bound, indicating quenching of fluorescence in the bound configuration and a value of $\Phi_1 / \Phi_2 = 0.83$.

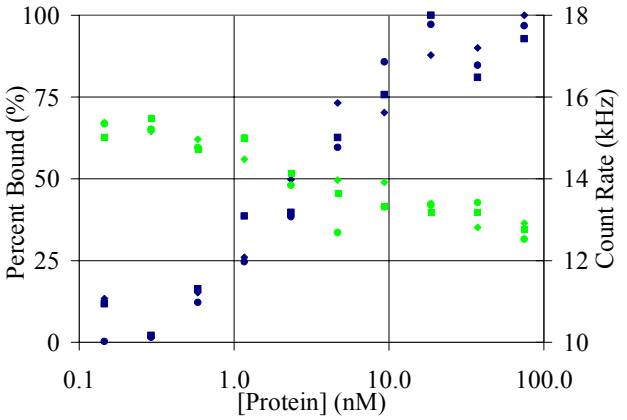

Fig. (**12**): The percentage of the ACF with the bound diffusional residence time (blue points, left scale) and the count rate (green points, right scale) for three 30 s FCS measurements at points from the binding isotherm titration of Fig. (**9**) of 1.1 nM Alexa-488-labeled Bak versus Bcl-x_L receptor protein.

Eqns. (5), (6), (7), and (10) may be manipulated obtain the fractional concentration of bound species $N_1/(N_1+N_2)$ from the fractional contribution to the ACF $c_1/(c_1+c_2)$ and the relative fluorescence brightness Φ_1/Φ_2 of bound and free species as

$$\frac{N_1}{N_1+N_2}=\left[1+\left(\frac{\Phi_1}{\Phi_2}\right)^2\left(\left(\frac{c_1}{c_1+c_2}\right)^{-1}-1\right)\right]^{-1}. \qquad (12)$$

Fig. (**13**) shows the percentage of bound ACF component $c_1/(c_1+c_2)\times 100\%$ obtained by averaging the 3 independent measurements of Fig. (**12**) (blue diamond points), the percentage concentration of bound labeled-ligand $N_1/(N_1+N_2)\times 100\%$, obtained by use of Eqn. (12) to account for the fluorescence quenching factor $\Phi_1/\Phi_2 = 0.83$ (green triangle points), together with a curve fit to the binding isotherm, which yields a dissociation constant of $K_d \approx 1.5$ nM, in approximate agreement with the result obtained by FP in Fig. (**9**). Fig. (**13**) also shows that if the correction for the 83% fluorescence quenching were omitted, a value of $K_d \approx 2.3$ nM would be obtained. The perfect agreement between the later value and the result from FP in Fig. (**9**), which was obtained at a different temperature, is coincidental, and the difference between the FP result of 2.3 nM and the FCS result of 1.5 nM is comparable to the typical level of accuracy and precision of such assays.

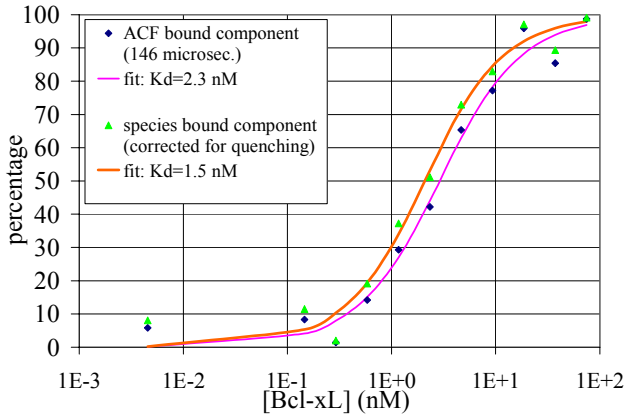

Fig. (**13**): FCS assay of binding isotherm titration of Bcl-x_L receptor protein for a constant 1.1 nM concentration of Alexa-488-labeled Bak.

The results of Fig. (**13**) illustrate that FCS can be successfully applied to quantitative ligand binding assays. In this particular example, FP proved to be simple, rapid, and accurate for determining the affinity of non-fluorescent ligands by equilibrium competition binding [58]. FP was chosen for screening because assay components similar to these were abundant and automated high-throughput FP methodology was available and well established. However, in many other cases the supply of target protein is limited and the relatively challenging labeling and bio-activity requirements that must be satisfied for a successful FP binding assay [30] that is also sufficiently robust under screening conditions, are not readily achieved. In such situations the FCS approach is a practical and versatile alternative to turn to.

ABBREVIATIONS

ACF	autocorrelation function
CPU	central processor unit (in reference to a computer)
FCS	fluorescence correlation spectroscopy
FCCS	fluorescence cross-correlation spectroscopy
FIDA	fluorescence intensity distribution analysis
FILDA	fluorescence intensity and lifetime analysis
FIMDA	fluorescence intensity multiple distribution analysis

FP	fluorescence polarization
PC	personal computer
PCH	photon counting histogram
SIMD	single instruction multiple data
SMD	single-molecule detection
SPIDA	successive photon interval density analysis
TOA	time of arrival (in reference to a photon)

REFERENCES

[1] Magde D.; Elson E.L. and Webb W.W. (1972) *Phys. Rev. Lett.*, **29**, 705-708.
[2] Elson, E.L. and Magde, D. (1974) *Biopolymers*, **13**, 1-27.
[3] Magde, D.; Webb, W.W. and Elson, E.L. (1974) *Biopolymers*, **13**, 29-61.
[4] Ehrenberg, M. and Rigler, R. (1974) *Chem. Phys.*, **4**, 390-401.
[5] Berne, B.J. and Pecora, R., (1976) *Dynamic light scattering*, Wiley, New York (esp. Sec. 6.6).
[6] Aragón, S.R. and Pecora, R. (1976) *J. Chem. Phys*., **64**, 1791-1803.
[7] Magde, D.; Webb, W.W. and Elson, E.L., 1978, *Biopolymers*, **17**, 361-376.
[8] Shera, E.B.; Seitzinger, N.K.; Davis, L.M.; Keller, R.A. and Soper, S.A. (1990) *Chem. Phys. Lett.***, 174**, 553-557.
[9] Qian, H. and Elson, E.L., (1991) *Applied Optics*, **30**, 1185-1195.
[10] Rigler, R.; Widengren, J. and Mets, Ü. (1992) in *Fluorescence Spectroscopy: New Methods and Applications*, (Wolfbeis, O.S, Ed.), Springer-Verlag, Berlin, pp. 13-24.
[11] Rigler, R.; Mets, Ü.; Widengren, J. and Kask P (1993) *Eur. Biophys. J.*, **222**, 169-175.
[12] Li, L.Q. and Davis, L.M. (1993) *Rev. Sci. Instrum*., **64**, 1524-1529.
[13] Mets Ü. and Rigler R (1994) *J. Fluorescence*, **4**, 259-263.
[14] Eigen, M. and Rigler, R., (1994) *Proc. Natl. Acad. Sci. USA*, **91**, 5740-5747.
[15] Nie, S.; Chiu, D.T. and Zare, R.N. (1994) *Science*, **266**, 1018-1021.
[16] Berland, K.M., So, P.T. and Gratton, E. (1995) *Biophys. J.*, **68**, 694-701.
[17] Spinelli, A.; Davis, L.M. and Dautet, H. (1996) *Rev. Sci. Instrum*., **67**, 55-61.
[18] Thompson, N.L. (1991) in *Topics in Fluorescence Spectroscopy, Vol. 1: Techniques*, (Lakowicz, J.R., Ed.), Plenum Press, New York, pp. 337-378.
[19] Kinjo M. and Rigler R. (1995) *Nuc. Acid. Res.*, **23**, 1795-1799.
[20] Jankowski, T. and Janka, R. (2001) *ibidem* [21], pp. 331-345.
[21] (2001) *Fluorescence Correlation Spectroscopy: Theory and Applications*, (Rigler, R. and Elson, E.S., Eds.), Springer, Berlin.
[22] Visser, A.J.W.G. and Hink, M.A. (1999) *J. Fluorescence*, **9**, 81-87.
[23] Webb, W.W. (2001) *Appl. Opt.*, **40**, 3969-3983; and *ibidem* [21], pp. 305-330.
[24] Widengren, J. and Mets, Ü. (2002) in *Single Molecule Detection in Solution*, (Zander, C.; Enderlein, J. and Keller, R.A., Eds.), Wiley-VCH Verlag, Berlin, pp. 69-120.
[25] Davis, L.M.; Ball, D.A.; Williams, P.E.; Matayoshi, E.D. and Swift, K.M. (2003) in SPIE Proc. Vol. 4966 *Microarrays and Combinatorial Technologies for Biomedical Applications*, (Nicolau, D.V. and Raghavachari, R. Eds.) SPIE, Bellingham, WA, pp. 117-128.
[26] Sittampalam, G.S.; Kahl, S.D. and Janzen, W.P. (1998) *J. Clinical Ligand Assay*, **21**, pp. 239-246.
[27] Swift, K.; Anderson, S.N. and Matayoshi, E (2001) in SPIE Proc. Vol. 4252 *Advances in Fluorescence Sensing Technology V*, (Lakowicz, J.R. and Thompson, R.B. Eds.) SPIE, Bellingham, WA, pp. 47-58.

[28] Moore, K.J.; Turconi, S.; Ashman, S.; Ruediger, M.; Haupts, U.; Emerick, V. and Pope, A.J. (1999) *J. Biomolecular Screening*, **4**, pp. 335-353.
[29] Koltermann, A.; Kettling, U.; Bieschke, J.; Winkler, T. and Eigen, M. (1998) *Proc. Natl. Acad. Sci. USA*, **95**, 1421-1426.
[30] Matayoshi, E. and Swift, K. (2001) *ibidem* [21], pp. 84-98.
[31] Meseth, U.; Wohland, T.; Rigler, R. and Vogel, H. (1999) *Biophys. J.*, **76**, pp. 1619-1631.
[32] Swift, K. and Matayoshi, E. (1995) in SPIE Proc. Vol. 2388 *Advances in Fluorescence Sensing Technology II*, (Lakowicz, J.R. Ed.) SPIE, Bellingham, WA, pp. 182-189.
[33] Chan, Y.; Muller, J.D.; So, P.T.C. and Gratton, E. (1999) *Biophys. J.*, **77**, pp. 553-567.
[34] Kask, P.; Palo, K.; Ullmann, D. and Gall, K. (1999) *Proc. Natl. Acad. Sci. USA* **6**, pp. 13756-13761.
[35] Palo, K.; Mets, Ü; Jäger, S.; Kask, P. and Gall, K. (2000) *Biophys. J.*, **79**, pp. 2858-2866.
[36] Eggeling, C. (2003) *this issue*.
[37] Brock, R., Hink, M.A. and Jovin, T.M. (1998) *Biophys. J.*, **75**, pp. 2547-2557.
[38] Widengren, J.; Mets, Ü and Rigler, R. (1995) *J. Phys. Chem.*, **99**, 13368-13379.
[39] Tetin, S.Y.; Swift, K.M. and Matayoshi, E.D. (2002) *Anal. Biochem.*, **307**, 84-91.
[40] Berland, K. and Shen, G. (2003) SPIE Proc. Vol. 4963 *Multiphoton Microscopy in the Biomedical Sciences III*, (Perisamy, A. and So, P.T.C. Eds.) SPIE, Bellingham, WA, pp. 1-12.
[41] Hess, S.T. and Webb, W.W. (2002) *Biophys. J.*, **83**, 2300-2317.
[42] Bunfield, D.H. and Davis, L.M. (1998) *Appl. Opt.*, **37**, 2315-2326.
[43] Wohland, T.; Rigler, R. and Vogel, H. (2001) *Biophys. J.*, **80**, pp. 2987-2999.
[44] Davis, L.M.; Williams, P.E.; Cain, H.M.; Ball, D.A.; Parigger, C.G.; Matayoshi, E.D. and Swift, K.M. (2002) *Biophys. J.*, **82**, p. 43a.
[45] Gerber, R. (2002) *The Software Optimization Cookbook*, Intel Press, Hillsboro, Oregon (ISBN 0-9712887-1-2).
[46] Schatzel, K. (1993) in *Dynamic Light Scattering*, (W. Brown, Ed.) Clarendon Press, Oxford, pp. 76-148.
[47] Li, L.Q. and Davis, L.M. (1995) *Appl. Opt.*, **34**, 3208-3217.
[48] Eid, J.S.; Müller, J.D. and Gratton, E. (2000) *Rev. Sci. Instrum.*, **71**, 361-368.
[49] Davis, L.M.; Williams, J.G.K. and Lamb, D.T. (1999) SPIE Proc. Vol. 3570 *Biomedical Sensors, Fibers, and Optical Delivery Systems*, (Baldini, F.; Croitoru, N.I.; Frenz, M.; Lundstrom, I.; Miyagi, M.; Pratesi, R. and Wolfbeis, O.S. Eds.) SPIE, Bellingham, WA, pp. 282-293.
[50] Saffarian, S. and Elson, E.L. (2003) *Biophys. J.*, **84**, 2030-2042.
[51] Jakeman, E.; Pike, E.R. and Swain, S. (1971) *J. Phys. A: Gen. Phys.*, **4**, 517-534.
[52] Koppel, D.E. (1974) *Phys. Rev. A*, **10**, 1938-1945.
[53] Qian, H. (1990) *Biophys. Chem.*, **38**, 49-57.
[54] Kask, P., Gunther, R. and Axhausen, P. (1997) *Eur. Biophys. J.*, **25**, 163-169.
[55] Schatzel, K.; Drewel, M. and Stimac, S. (1988) *J. Mod. Optics*, **35**, 711-718.
[56] Fesik, S.W. and Shi, Y. (2001) *Science*, **294**,1477-1478.
[57] Sattler, M.; Liang, H.; Nettesheim, D.; Meadows, R.P.; Harlan, J.E.; Eberstadt, M.; Yoon, H.S.; Shuker, S.B.; Chang, B.S.; Minn, A.J.; Thompson, C.B. and Fesik, S.W. (1997) *Science*, **275**, 983-986.
[58] Petros, A.M.; Nettesheim, D.G.; Wang, Y.; Olejniczak, E.T.; Meadows, R.P.; Mack, J.; Swift, K.; Matayoshi, E.D.; Zhang, H.; Thompson, C.B. and Fesik, S.W. (2000) *Protein Science*, **9**, pp. 2528-2534.